AD_____

Award Number: DAMD17-98-1-8068

TITLE: A Novel Ultrasonic Imaging Method for Remote Palpation of Breast Tissues

PRINCIPAL INVESTIGATOR: Gregg Trahey, Ph.D.

CONTRACTING ORGANIZATION: Duke University
Durham, North Carolina 27708-0282

REPORT DATE: September 1999

TYPE OF REPORT: Annual

PREPARED FOR: U.S. Army Medical Research and Materiel Command
Fort Detrick, Maryland 21702-5012

DISTRIBUTION STATEMENT: Approved for public release
distribution unlimited

The views, opinions and/or findings contained in this report are those of the author(s) and should not be construed as an official Department of the Army position, policy or decision unless so designated by other documentation.

20001020 044

DTIC QUALITY INSPECTED 4

REPORT DOCUMENTATION PAGE

Form Approved
OMB No. 074-0188

Public reporting burden for this collection of information is estimated to average 1 hour per response, including the time for reviewing instructions, searching existing data sources, gathering and maintaining the data needed, and completing and reviewing this collection of information. Send comments regarding this burden estimate or any other aspect of this collection of information, including suggestions for reducing this burden to Washington Headquarters Services, Directorate for Information Operations and Reports, 1215 Jefferson Davis Highway, Suite 1204, Arlington, VA 22202-4302, and to the Office of Management and Budget, Paperwork Reduction Project (0704-0188), Washington, DC 20503

1. AGENCY USE ONLY (Leave blank)	2. REPORT DATE September 1999	3. REPORT TYPE AND DATES COVERED Annual (01 Sep 98 - 31 Aug 99)

4. TITLE AND SUBTITLE 6. AUTHOR(S) Gregg Trahey, Ph.D.	5. FUNDING NUMBERS
7. PERFORMING ORGANIZATION NAME(S) AND ADDRESS(ES) Duke University Durham, North Carolina 27708-0282	8. PERFORMING ORGANIZATION REPORT NUMBER

9. SPONSORING / MONITORING AGENCY NAME(S) AND ADDRESS(ES) U.S. Army Medical Research and Materiel Command Fort Detrick, Maryland 21702-5012	10. SPONSORING / MONITORING AGENCY REPORT NUMBER

11. SUPPLEMENTARY NOTES

12a. DISTRIBUTION / AVAILABILITY STATEMENT Approved for public release	12b. DISTRIBUTION CODE

13. ABSTRACT (Maximum 200 Words)

A method of Remote Palpation, which may allow the detection of small, stiff lesions lying deep within the breast is under investigation. In this method, acoustic radiation force applied to localized (approximately 2 mm^3) regions of tissue, and the resulting tissue displacements are mapped using ultrasonic correlation based methods. An area that is stiffer than the surrounding medium distributes the force, resulting in larger regions of disp,lacement, and smaller maximum displacements. The resulting displacement maps may be used to image tissue stiffness.

We have developed a finite element model of Remote Palpation, with which a parametric analysis of the affect of varying tissue and acoustic beam characteristics on radiation force induced tissue displacements has been performed. We have developed phantom tissue fabrication facilities, with which models of tissue of varying stiffness and acoustic absorption characteristics have been built. Experimental pulse sequences have been developed for our Elegra scanner, with which initial experiments have been performed in phantoms. The tissue displacement patterns observed in the experiments are consistent with those predicted by the simulations. Peak displacements of 30 microns were observed in a phantom with a Young's modulus of 0.8 kPa. These initial results suggest considerable clinical potential for Remote Palpation.

14. SUBJECT TERMS 1. Breast Cancer 2. Acoustic Radiation Force 3. Ultrasound Phantoms 4. Tissue Young's modules 5. Elastography	15. NUMBER OF PAGES 45
	16. PRICE CODE

17. SECURITY	18. SECURITY	19. SECURITY	20. LIMITATION OF
Unclassified	Unclassified	Unclassified	Unlimited

FOREWORD

Opinions, interpretations, conclusions and recommendations are those of the author and are not necessarily endorsed by the U.S. Army.

____ Where copyrighted material is quoted, permission has been obtained to use such material.

____ Where material from documents designated for limited distribution is quoted, permission has been obtained to use the material.

____ Citations of commercial organizations and trade names in this report do not constitute an official Department of Army endorsement or approval of the products or services of these organizations.

____ In conducting research using animals, the investigator(s) adhered to the "Guide for the Care and Use of Laboratory Animals," prepared by the Committee on Care and use of Laboratory Animals of the Institute of Laboratory Resources, national Research Council (NIH Publication No. 86-23, Revised 1985).

____ For the protection of human subjects, the investigator(s) adhered to policies of applicable Federal Law 45 CFR 46.

____ In conducting research utilizing recombinant DNA technology, the investigator(s) adhered to current guidelines promulgated by the National Institutes of Health.

____ In the conduct of research utilizing recombinant DNA, the investigator(s) adhered to the NIH Guidelines for Research Involving Recombinant DNA Molecules.

____ In the conduct of research involving hazardous organisms, the investigator(s) adhered to the CDC-NIH Guide for Biosafety in Microbiological and Biomedical Laboratories.

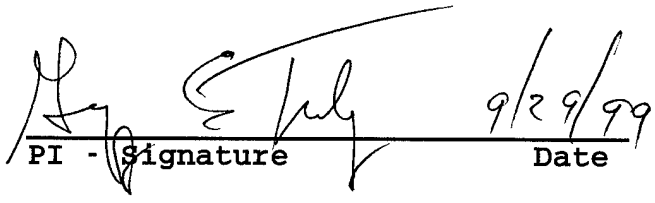

PI - Signature Date

Contents

1 Front Cover 1

2 Standard Form 298 2

3 Foreword 4

4 Table of Contents 5

5 Introduction 6

6 Body 6

7 Key Research Accomplishments 7

8 Reportable Outcomes 8

9 Conclusions 8

10 Bibliography 10

11 Appendices 11

11.1 Figures 11

11.2 Finite Element Model Paper 13

5 Introduction

The early detection of breast cancer reduces patient mortality. The most common method of breast cancer detection is palpation. However, lesions that lie deep within the breast are difficult to palpate when they are small.Thus, a method of Remote Palpation, which may allow the detection of small lesions lying deep within the breast, is currently under investigation. In this method, acoustic radiation force is used to apply localized (on the order of 2 mm^3) forces within tissue, and the resulting tissue displacements are mapped using ultrasonic correlation based methods. An area that is stiffer than the surrounding medium distributes the force, resulting in larger regions of displacement, and smaller maximum displacements. The resulting displacement maps may be used to image tissue stiffness. In the first year of support, we have developed a finite element model that predicts tissue displacement patterns resulting from the application of acoustic radiation force. We have developed phantom tissue fabrication facilities in order to design phantoms to validate the finite element model, and we have developed pulsing sequences for our Elegra ultrasound scanner with which we have performed initial validation experiments.

6 Body

We have developed a finite element model of Remote Palpation, with which we have determined the necessary acoustic parameters to generate detectable displacements *in vivo*. The findings are summarized in Appendix 11.2, which is a preprint of a paper we have submitted to *Ultrasonic Imaging*. This represents completion of items 1, 2, 3, and 5 listed under task 1 in the Statement of Work.

It was determined that experimental validation of the model requires investigation of phantoms with varying stiffnesses, and it was not practical to procure multiple phantoms. Therefore, we have developed an ultrasound phantom fabrication facility in our laboratory. Using validated recipes for ultrasonic elastography phantoms [1], we now have the capability to design and build custom phantoms. We have access to a rheometer, which allows calibration of the Young's modulus of these phantoms. In addition, we are currently developing the required experimental apparatus to calibrate the acoustic properties (*i.e.* absorption and sound speed) of the phantoms. This phantom fabrication and calibration facility fulfills the

first item listed under task 2 in the Statement of Work.

An initial experimental pulse sequence for Remote Palpation implementation has been developed in accordance with the findings presented in Appendix 11.2. This sequence provides a single focal location for the application of radiation force. First, a series of low intensity, spatially distributed 'tracking lines' are fired and stored for reference. Then a series of high intensity 'pushing lines' are fired along a single line of flight in the center of the tracking lines. These pushing lines are fired for 10 milliseconds. Finally, another series of tracking lines are fired. These tracking lines are interspersed with pushing lines, in order to avoid relaxation of the tissue. This sequence is then repeated eleven times, and the data is stored for off-line processing. This processing is performed using MATLAB. Each tracking line is divided into sequential axial search regions, and the cross correlation between the reference lines and tracking lines is computed in order to determine the tissue motion in each region. Correlation based methods are the accepted standard for tracking displacements in sequential ultrasonic images [4, 3, 6]. This experimental implementation represents partial completion of item 3, task 2 in the Statement of Work.

Figures 1 and 2 illustrate the first experimentally obtained Remote Palpation images. Figure 2 portrays the displacement through time at the focal point of the transducer. This temporal response is consistent with that predicted by the simulations. Figure 1 illustrates the displacement maps generated by implementing the above pulse sequence in a custom designed 0.8 kPa phantom, which models normal breast tissue. The pattern is consistent with those from the finite element model. Correlation with the simulation results is not yet possible due to the lack of calibration of the acoustic properties of this phantom. We have measured the intensities used during experimental implementation of Remote Palpation (item 2 under Task 2 in the statement of work). However, when using high pressure amplitude pulses some challenges exist with respect to differences in nonlinear propagation between water (where calibrated pressure measurements are made) and our phantoms. We are working to overcome these challenges.

7 Key Research Accomplishments

1) Developed finite element model of radiation force induced tissue motion.
2) Performed parametric analysis of the effect of varying tissue and acoustic properties on tissue displacements.

3) Developed an initial experimental pulse sequence to implement Remote Palpation using results from simulations as a guide.

4) Developed phantom fabrication facilities in order to design calibrated elastography phantoms.

5) Built an elastography phantom of normal tissue, with a Young's modulus of 0.8 kPa.

6) Measured the intensity fields generated by our Elegra ultrasound scanner when using our experimental pulse sequence.

7) Implemented Remote Palpation on phantom, and generated displacement maps consistent with the simulated results.

8 Reportable Outcomes

1) Paper submission to *Ultrasonic Imaging*, entitled: "A finite element model of Remote Palpation of breast lesions using radiation force: factors affecting tissue displacement."

2) Presentation at the Twenty-third international symposium on ultrasonic imaging and tissue characterization in Arlington, Va (May 28, 1998) entitled: "The use of radiation force induced tissue displacements to image stiffness: a feasibility study."

3) Presentation at the 1999 IEEE International Ultrasonics symposium at Lake Tahoe, NV (October 19, 1999) entitled: "Finite element analysis of radiation force induced tissue motion."

9 Conclusions

The clinical implications of the results obtained during the first year of support are promising. The simulations and initial experimental results appear to be consistent, and provide the framework for the design of a Remote Palpation imaging system. For a clinically relevant range of elastic moduli and lesion sizes, considerably different displacement patterns were simulated. The simulations indicate that the acoustic intensity requirements for Remote Palpation increase with tissue stiffness. Given the considerable variation in the reported

range of Young's moduli for breast tissue [2, 5] it may be that a more powerful transducer is required for clinical implementation. Displacements of up to 30 microns were observed experimentally in a fairly compliant homogeneous phantom (Young's modulus of 0.8 kPa). The results indicate that lesions as small as 5 mm in diameter could be detected using Remote Palpation, which could have considerable clinical impact. Key issues requiring further investigation prior to clinical implementation include: thermal and power issues, development of phantoms with lesions, and investigation of methods of information display.

10 Bibliography

References

[1] T. Hall, M. Bilgen, M. Insana, and P. Chaturvedi. Phantoms for elastography. In *Proceedings of the 1996 Ultrasonics Symposium*, pages 1193–1196, 1996.

[2] T. Krouskop, T. Wheeler, F. Kallel, B. Garra, and T. Hall. Elastic moduli of breast and prostate tissues under compression. *Ultrasonic Imaging*, 20:260–274, 1998.

[3] M. O'Donnell, A. Skovoroda, B. Shapo, and S. Emelianov. Internal displacement and strain imaging using ultrasonic speckle tracking. *IEEE Trans. Ultrason., Ferroelec., Freq. Contr.*, 41:314–325, 1994.

[4] J. Ophir, I. Cespedes, H. Ponnekanti, Y. Yazdi, and X. Li. Elastography: A quantitative method for imaging the elasticity of biological tissues. *Ultrasonic Imaging*, 13:111–134, 1991.

[5] A. Skovoroda, A. Klishko, D. Gusakyan, Y. Mayevskii, V. Yermilova, G. Oranskaya, and A. Sarvazyan. Quantitative analysis of the mechanical characteristics of pathologically changed soft biological tissues. *Biophysics*, 40(6):1359–1364, 1995.

[6] G. Trahey, J. Allison, and O. Vonramm. Angle independent ultrasonic detection of blood flow. *IEEE Trans. Biomed. Egr.*, BME-34(12):965–967, 1987.

11 Appendices

11.1 Figures

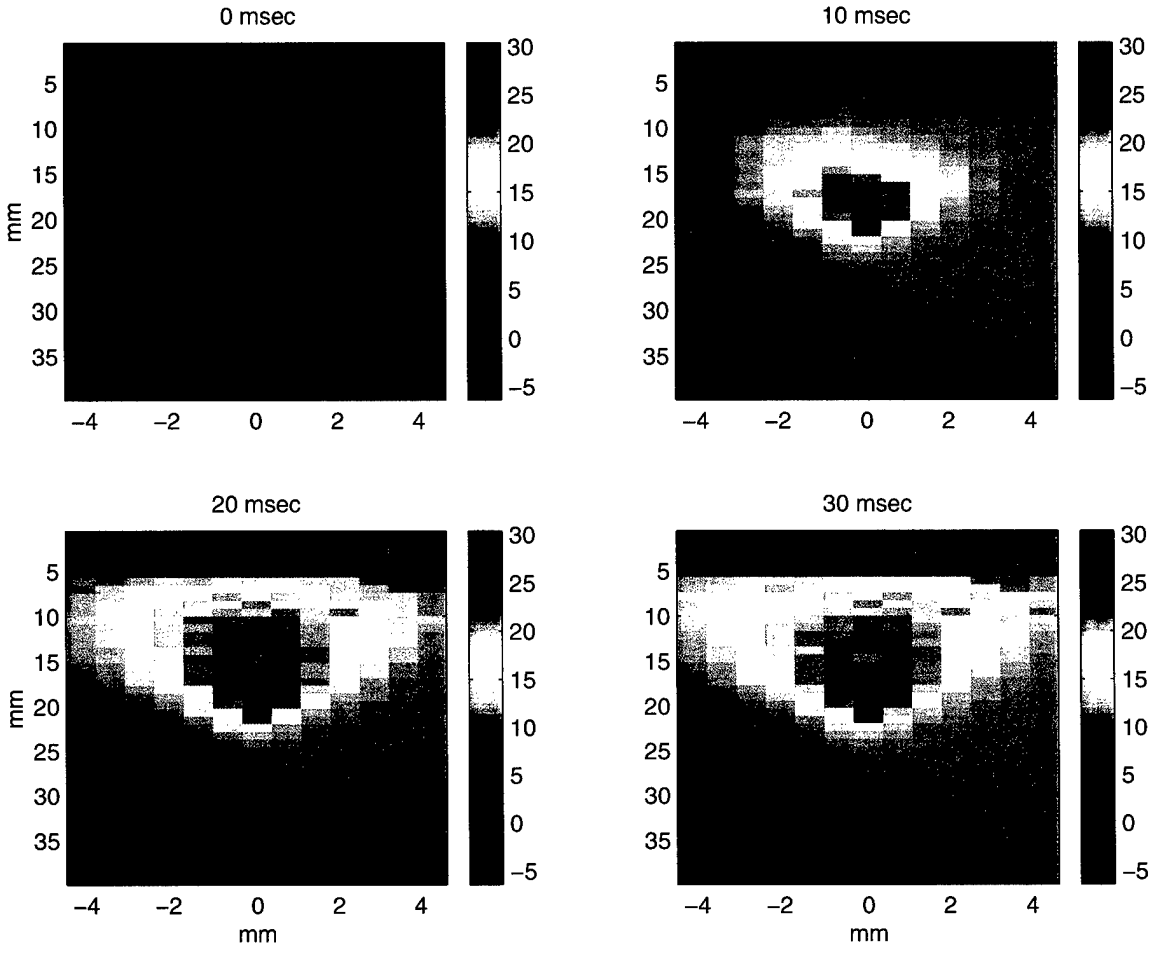

Figure 1: Initial Remote Palpation displacement maps generated using a modified commercial diagnostic ultrasound scanner (Elegra, Siemens Medical Systems, Ultrasound Group, Issaquah, WA) and a tissue mimicking phantom. The transducer is at the top of each image, and the different maps show changes in the displacement profile over time. The tissue mimicking material had a stiffness of 0.8 kPa. These maps show a large displacement near the focal region (20 mm on the y-axis). The scale for the displacements in microns, with 28 microns being the maximum displacement.

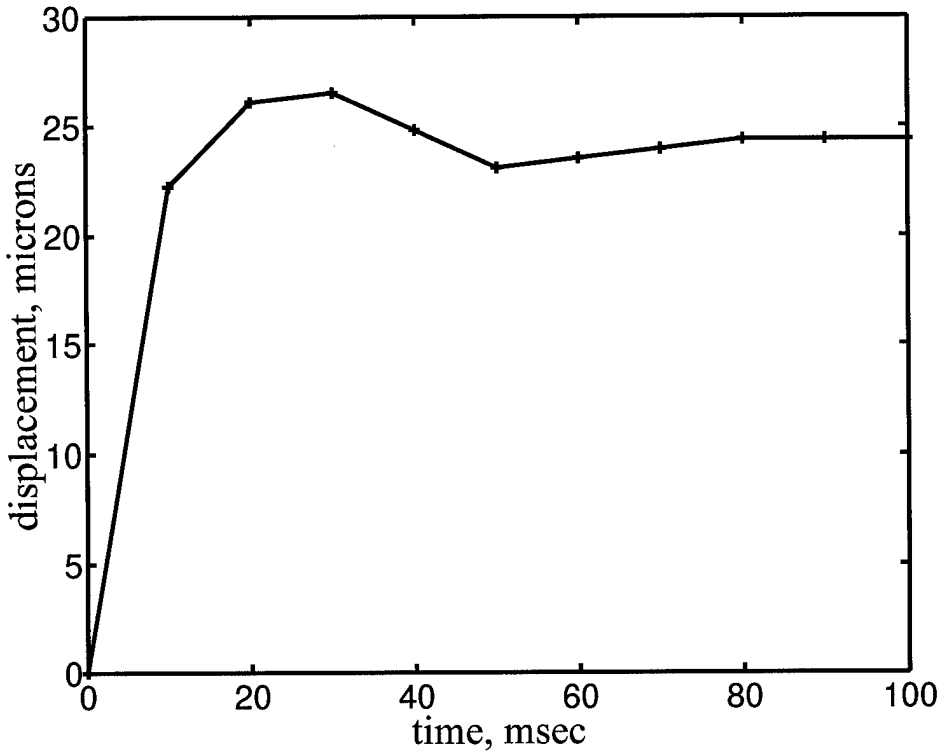

Figure 2: Displacement through time at the focal point of the transducer. This temporal response is consistent with that predicted by the simulations, in that there is a large initial displacement within the first 10 milliseconds, and then the pattern asymptotes to a maximum displacement. The slight ringing observed between 20 and 60 milliseconds suggests that the phantom material is slightly under-damped, which was not observed in the simulations due to the application of numerical damping.

11.2 Finite Element Model Paper

A Finite Element Model of Remote Palpation of Breast Lesions Using Radiation Force: Factors Affecting Tissue Displacement

Kathryn R. Nightingale[1], Roger W. Nightingale[1], Mark L. Palmeri[1], and Gregg E. Trahey[1,2]

[1]Duke University Department of Biomedical Engineering
[2]Duke University Medical Center, Department of Radiology
Durham, NC 27708
krn@acpub.duke.edu

September 29, 1999

Abstract

The early detection of breast cancer reduces patient mortality. The most common method of breast cancer detection is palpation. However, lesions that lie deep within the breast are difficult to palpate when they are small. Thus, a method of Remote Palpation, which may allow the detection of small lesions lying deep within the breast, is currently under investigation. In this method, acoustic radiation force is used to apply localized (on the order of 2 mm^3) forces within tissue, and the resulting tissue displacements are mapped using ultrasonic correlation based methods. An area that is stiffer than the surrounding medium distributes the force, resulting in larger regions of displacement, and smaller maximum displacements. The resulting displacement maps may be used to image tissue stiffness.

A Finite Element Model (FEM) of acoustic remote palpation is presented in this paper. Using this model, a parametric analysis of the affect of varying tissue and acoustic beam characteristics on radiation force induced tissue displacements is performed. The results are used to evaluate the resolution and contrast of acoustic remote palpation. The potential for using a single diagnostic transducer to both generate radiation force and track the resulting displacements is investigated.

Introduction

The early detection of breast cancer has been shown to significantly improve patient survival. Present methods of breast cancer detection include screening mammography and palpation, either by patient self-examination or clinical breast exam. Palpation relies on the manual detection of differences in tissue stiffness between breast lesions and normal breast tissue. The success of palpation is due to the fact that the elastic modulus (or Young's modulus) of malignant tumors is often an order of magnitude greater than that of normal breast tissue [1, 2], i.e. cancerous lesions feel 'harder' or 'stony' as compared to normal breast tissue.

This difference in Young's moduli is the basis for the investigation of imaging modalities that provide information about the stiffness of tissue. Traditionally, these have fallen into two categories, 1) sonoelasticity, in which low frequency shear wave propagation is imaged using Doppler methods, from which the elastic modulus (Young's modulus) of tissue can be estimated [3, 4, 5, 6, 7] and 2) elastography, in which local variations in tissue strain are determined by measuring local displacements that occur during global tissue compression [1, 8, 9]. A review of these methods is provided by Gao *et. al.* [10].

Recently, several authors have proposed the use of ultrasonic radiation force to remotely characterize tissue stiffness [11, 12, 13, 14, 15]. These methods propose the use of radiation force to displace tissue in a remote location, however they differ in the processing of the resulting information. The method under investigation herein is called Remote Palpation. In this method, acoustic radiation force is used to apply localized (on the order of 2 mm^3) forces within tissue, and the resulting tissue displacements are mapped using ultrasonic correlation based methods. An area that is stiffer than the surrounding medium distributes the force, resulting in larger regions of displacement, and smaller maximum displacements. If a single diagnostic transducer can be used to both generate radiation force and track the resulting displacements, Remote Palpation may have considerable clinical potential. This would provide ease of clinical implementation, as well as allowing the correlation between conventional B-mode images and Remote Palpation images.

The purpose of the work presented here is to investigate the potential for using acoustic radiation force to characterize localized variations in tissue stiffness, and specifically to identify the limits of resolution and contrast for Remote Palpation. Finite Element Methods (FEM) are used for this investigation, which allow the performance of a parametric analysis

of varying tissue and acoustic beam parameters. The parameters that are studied include: acoustic beam intensity, transducer design and f-number, tissue stiffness, lesion size, and lesion stiffness. These results will be used to guide the design of future Remote Palpation experiments.

Background

Acoustic radiation force is a phenomenon associated with the propagation of acoustic waves through a dissipative medium. It is caused by the energy density gradient that occurs in the medium, arising either from absorption or reflection of the wave. This gradient results in the application of a force in the direction of wave propagation [16]. In an absorbing medium, and under plane wave assumptions, this force can be represented by the following equation [16, 17, 18, 19]:

$$F = \frac{W_{absorbed}}{c} = \frac{2\alpha I}{c}, \tag{1}$$

where F is acoustic radiation force [kg/(s^{2}cm^2)], or [dynes/(1000 cm^3)], $W_{absorbed}$ [Watts/(100 cm^3)] is the power absorbed by the medium at a given point in space, c [m/s] is the speed of sound in the medium, α [m^{-1}] is the absorption coefficient of the medium, and I [Watts/cm^2] is the temporal average intensity at a given point in space. Equation 1 provides a simple relationship between the temporal average intensity of an acoustic beam, and the resulting radiation force (which is in the form of a body force, or force per unit volume). A direct relationship between F and frequency is implied by the dependence on α, which increases with frequency.

Equation 1 can be used to model radiation force fields associated with complex intensity field geometries by computing or measuring the temporal average intensity at each point in a three dimensional region of interest. The axial extent of most intensity fields is roughly dependent upon transducer focal configuration, which is generally indicated by the transducer f-number:

$$fnumber = \frac{z}{D}, \tag{2}$$

where z is the acoustic focal length and D is the aperture width. Therefore, the transducer configurations under investigation herein are differentiated by f-number throughout this paper. In referring to varying f-number transducers, the notation F/n is used, where n is the number. For example, a transducer with an f-number of 2 is referred to as an F/2 configuration.

In order to determine the effect that a specific radiation force field will have on a given

tissue type, one can solve the equations of motion under the appropriate initial conditions and boundary conditions. The motion resulting from these force fields when applied to a fluid contained within spherical boundaries has been successfully computed by numerically solving the Navier-Stokes equations [20]. The work presented herein involves similar force fields applied to elastic media.

Methods

The finite element model of Remote Palpation presented herein determines tissue displacements resulting from the application of radiation force generated by various diagnostic transducer configurations. Model implementation is performed using a two step approach: first the spatially distributed intensity field from a given transducer and set of transmit parameters is determined and the associated radiation force field is computed using Equation 1. Second, finite element methods are used to solve for the resulting tissue displacement patterns.

In order to determine the acoustic intensity field distribution associated with various diagnostic transducer configurations that might be used in Remote Palpation (*i.e.* linear and multi-row arrays with varying aperture widths), the temporal average intensity fields corresponding to these transducers were modeled using FIELD_II (http://www.it.dtu.dk/~jaj/field/) [21], an acoustic field simulation software program. This program allows the accurate modeling of intensity fields from arbitrarily shaped transducer arrays. Two transducers were modeled: the Siemens 75L40 linear transducer (one row of elements, center frequency 7.2 MHz, element height 5 mm, aperture width dependent upon the number of active elements; Siemens Medical Systems, Ultrasound Group, Issaquah, WA), and a two-dimensional 8x128 element custom diagnostic transducer developed for our research scanner (8 rows of elements, center frequency 7.2 MHz, element height 1.45mm, aperture width determined by the number of active elements in both dimensions; Tetrad Corp., Englewood CO). Throughout this paper, these will be referred to as the linear transducer and the 2D transducer, respectively. The simulated voltage used to excite each element was fixed; thus, for a given element size, when more elements were excited, more energy was transmitted. Both transducers were focused laterally at the location of their elevation focal point (which was determined by their lens). The linear transducer had a fixed elevation f-number, and the lateral f-numbers were varied between F/1 and F/3 by varying the number of active elements in the array. The 2D transducer was modeled using all of its elements (8x128), and thus had an F/2 elevation and F/1 lateral configuration.

The intensity fields for each transducer configuration (or f-number) were computed in the axial/lateral plane of the transducer, normalized, and discretized into three contours of constant intensity (see Fig. 1). Once these contours and the desired boundaries were in place, they were imported into a finite element mesh generation program (Hypermesh, Altair Computing Inc., Troy, MI). The mesh was generated within this plane, and then rotated 90 degrees around its central axis, in order to achieve a three dimensional model (Fig. 2). The model was constrained on the surface of the distal quarter of the hemisphere (opposite the transducer location), thus modeling a breast resting on a concave platform. Because the boundary conditions did not allow motion normal to the planar surfaces in Figure 2, symmetry assumptions hold, and solution of this mesh simulates motion in one quarter of the axi-symmetric three dimensional spherical model.

In order to determine the radiation force value to be applied within each intensity contour, the normalized contours were scaled to a peak value of 90 W/cm^2 for the linear, F/1 transducer configuration. Eq. (1) was then used, along with the tissue properties below, to convert the regions of constant intensity to regions of constant body force. The resulting maximum body force was 4882 $dynes/cm^3$.

The tissue properties (α, c, ρ_0, and E) were selected to model realistic *in vivo* values. The absorption coefficient of breast tissue was .415 cm^{-1}, or 3.6 dB cm^{-1} (recall that the center frequency was 7.2 MHz). The speed of sound was 1530 m s^{-1}, the density of tissue was 1000 kg m^{-3}, and the Young's modulus was 10 kPa. When lesions of varying stiffness were introduced, the Young's moduli ranged from 1 to 400 kPa, which is within the potential range of normal and diseased breast tissue [1, 2, 22]. The tissue was assumed to be elastic.

The equations of motion were then solved numerically using LS-DYNA (Livermore Software Technology Corporation, Livermore, CA). Radiation force was applied using a ramp and hold function, where the ramp up to the maximum force value was linear, occurring over 2 milliseconds, and the force was then applied continuously for 40 milliseconds. Numerical damping at twice the natural frequency of the system was introduced to reduce computation time for steady state analysis. This involved first solving the model without damping, computing the natural frequency of the system, and then solving the model again with damping. The same mesh was utilized for all simulations. Forces were applied to different mesh elements depending upon the transducer configuration, and tissue properties were applied to different elements depending upon the lesion size being modeled. There were 7440 elements in the mesh. The run times were anywhere from XX to YY minutes on a 450

MHz Pentium PC.

Results

In order to simplify the presentation of quantitative results, in many cases only the displacement profiles along the axial extent of the tissue are given, as computed at 20 milliseconds after force initiation (Figure 3, bottom row). This provides a reasonable interpretation of the differences in the displacement profiles because in the absence of a lesion, the lateral extent of the displacement profiles do not vary considerably for different tissue and transducer parameters.

The displacements in normal breast tissue are largest along the central axis of the transducer just in front of the focal point (first column of Figure 3). The peak displacement in this simulation was 2.8 microns, and the lateral extent of the motion (*i.e.* the lateral distance off axis where the displacement dropped to 50% of the peak) was 1.7 mm. The second column of Figure 3 provides the corresponding example when a 0.5 cm diameter lesion that is forty times more stiff than the surrounding tissue is present (*i.e.* Young's modulus of 400 kPa). Note that in this case, the lesion moves as a rigid body, and thus the lateral extent of the motion is much larger (3.9 mm), and the peak displacement is much smaller (0.9 microns). These figures suggest that clear, quantifiable differences exist between the displacement patterns generated in the presence or absence of a lesion.

Effect of Increasing Force: The simulations show a linear relationship between force and magnitude of displacement throughout the entire three-dimensional volume. Figure 4 illustrates peak displacement as a function of radiation force, clearly indicating that displacement increases linearly with force.

Effect of Breast Tissue Stiffness: Figure 5 indicates that the more stiff the baseline tissue is, the lower the maximum displacement will be for a given force. As is expected in an elastic medium, Figure 5 also shows that stiffness and displacement are inversely proportional to each other.

Effect of Transducer Configuration: For each transducer configuration, the shape of the displacement pattern in normal breast tissue was similar to the shape of the associated intensity field (Figure 6). Figure 7 illustrates the shape of the intensity fields produced by the various transducer configurations (*i.e.* the 0.1 level contour of Figure 1 for each

configuration), and Table 1 provides the normalized intensity values for each configuration. The axial displacement profiles generated by the different transducer configurations are presented in Figure 8. Both the largest peak displacement, and the smallest axial extent of the displacement profile were produced with the 2D transducer. For the linear transducer, the axial extent of the displacement profiles increased with increasing f-number, whereas the peak displacements decreased with increasing f-number. This trend was apparent in all but the comparison between the F/1 and F/1.5 cases, in which the profiles are similar along the axial extent of the F/1 profile, but the F/1.5 configuration exhibits a longer axial extent, with a larger maximum displacement.

Effect of Lesion Stiffness and Size: Figures 9 and 10 demonstrate the different displacement patterns associated with different lesion sizes and stiffnesses for the 2D transducer. Figures 11 and 12 provide the same information for the linear-F/1 transducer. Note that for both transducers, in the absence of a lesion, the dimensions of the displaced tissue follow the contours of the radiation force field, with the largest axial displacement near the focal point. In the presence of a lesion, the displacement patterns vary depending upon lesion size and Lesion-to-Tissue-Stiffness Ratio (LTSR). In the cases where the LTSR is 10 or more, the entire lesion is displaced as a rigid body. The larger the LTSR, the more uniform the displacement across the lesion becomes. For smaller lesions, the required LTSR for rigid body motion decreases.

There are considerable differences in the displacement patterns generated by the linear-F/1 and 2D transducer configurations for the 0.5 cm diameter lesion. The 2D intensity field is completely contained within the 0.5 cm diameter lesion, however the linear-F/1 intensity field extends beyond the lesion boundaries (Figure 7). The displacement profile for the linear-F/1 transducer exhibits a large displacement in front of the proximal lesion boundary, resulting from the material stiffness change within the intensity field (Figure 12). This effect is not present in the 2D case, where the intensity field is completely contained within the lesion (Figure 10).

A series of a simulations was also run in which both the breast tissue stiffness and the lesion stiffness were modified, but the LTSR was held constant (*i.e.* an LTSR of 10 was run for the following lesion and tissue stiffnesses, respectively: 100 and 10 kPa, 50 and 5 kPa, and 200 and 20 kPa). The LTSR's investigated were 10 and 20. Although the percent change in maximum displacement between normal breast tissue and the same tissue with an embedded lesion varied with the stiffness of the breast tissue, the trends with respect

to increasing LTSR were consistent. The greater the LTSR, the greater the difference in maximum displacements between the lesion and normal breast tissue cases.

Timing Issues: The response of tissue when exposed to radiation force is an initial large displacement followed by a slowly increasing or creeping displacement (Figure 13). The temporal extent of the initial large displacement varies with the presence or absence of a lesion, the size of the lesion, and the relative stiffness of the lesion and the surrounding tissue (LTSR). In order to quantify this initial ramp up time, an effective time constant is defined to be the time the tissue takes to reach 70% of its displacement at 20 milliseconds. This ranges from 2 to 5 milliseconds for the cases shown in Figure 13.

Another series of simulations was performed in which the force was removed after 20 milliseconds of application, in order to evaluate relaxation time. This set of simulations was run without damping. For the purpose of this discussion, the relaxation time is defined to be the time it takes for the displacement to decrease to 70% of its maximum value. Figure 14 portrays the relaxation times associated with normal breast tissue of varying stiffness. The results indicate that relaxation time decreases with increasing stiffness, with the shortest relaxation time being 0.2 milliseconds (E=18kPa) and the longest being 1 millisecond (E=1kPa).

Discussion

Both elastography methods and Remote Palpation are intended to image variations in tissue stiffness. Therefore, much of the research performed during the development of elastography is applicable to Remote Palpation, including: methods for information display, and measurements of tissue stiffness. The fundamental difference between the proposed Remote Palpation imaging method and elastography lies in the forcing function. In elastography, images of strain (the derivative of displacement) due to external, global force application are generated [1, 8, 9, 10]. In Remote Palpation, localized forces are generated deep within the tissue. This results in several potential advantages for the Remote Palpation method. Elastography images have been shown to suffer from signal decorrelation due to tissue compression (on the order of several hundred microns) [23], whereas the signal decorrelation resulting from Remote Palpation displacements (tens of microns) will be negligible. In addition, elastography imaging is susceptible to artifacts arising from varying boundary conditions. Because the forces used in Remote Palpation will be applied over small, localized volumes of tissue within the breast, the boundaries are effectively infinite.

The resolution of elastography systems is dependent upon several variables, including: transducer parameters, signal-to-noise ratio, pulse length and kernel size used for the tracking algorithm, the stiffness of tissue, and the size and relative stiffness of lesions (LTSR). In addition to the above factors, the resolution of Remote Palpation imaging systems will be dependent upon the shape and size of the intensity field (Figure 6). The simulations indicate that the smallest volumes of displaced tissue, as well as the largest peak displacements, are achieved with the 2D transducer in normal breast tissue. This was expected because this transducer has the smallest intensity field (Figure 7). In addition, the 2D transducer has more elements, which cover a larger surface area, thus the 2D transducer generates larger forces than the linear transducer (see Table 1). Where a 2D transducer is not available, the results indicate that an F/1 configuration is preferable, given its larger forces and smaller volumes as compared to larger f-number configurations.

Remote Palpation will be implemented clinically by multiple sequential applications of radiation force at different locations throughout a two-dimensional region of interest, using a single diagnostic transducer to both generate the required radiation force and track the resulting displacements. At each force location, a series of low intensity, spatially distributed 'tracking lines' will be fired and stored for reference. Then a series of high intensity 'pushing lines' will be fired along a single line of flight in the center of the tracking lines, which will be the source of the localized radiation force. These pushing lines will be fired for 5 milliseconds in order to accommodate the initial displacement ramp-up time (Figure 13). Finally, another series of tracking lines will be fired. These tracking lines will be interspersed with pushing lines, in order to avoid relaxation of the tissue, which will occur within a few milliseconds of the removal of radiation force (Figure 14). Each tracking line will be divided into sequential axial search regions, and the cross correlation between the reference lines and tracking lines will be computed in order to determine the tissue motion in each region. Correlation based methods are the accepted standard for tracking displacements in sequential ultrasonic images [8, 9, 24].

In the implementation of Remote Palpation, a significant issue is whether or not it is feasible to use a single transducer to both generate the radiation force and track the resulting displacements. This would be advantageous for several reasons. First, it would facilitate ease of clinical implementation, possibly as an option on conventional diagnostic systems. Second, it would allow direct correlation of Remote Palpation images with conventional B-mode images. Finally, it would avoid the considerable challenges associated with aligning multiple transducers. The primary challenge for single transducer implementation is generating

enough force to produce detectable displacements. The definition of a 'detectable displacement profile' is dependent upon the sensitivity of the displacement tracking algorithm. The theoretical lower limit on the distance that can be tracked using correlation based algorithms can be estimated using the Cramer-Rao Lower Bound [25]. Assuming a good Signal-to-Noise Ratio (40 dB), and a high correlation between the reference and tracking lines (0.998), the estimated lower limit on the distance that can be tracked during Remote Palpation is 0.5 microns. Therefore, in order to achieve reasonable resolution, peak displacements of at least five microns would be desirable.

The displacement magnitudes that will be achieved *in vivo* are clearly dependent upon the Young's modulus of breast tissue (Figure 5). This is a challenging parameter to characterize that has been attempted by only a few researchers. The reported numbers for normal breast tissue range from 1 to 18 kPa [1, 2, 22]. This variability suggests that the radiation force that will be necessary to achieve peak displacements of 5 microns in normal breast tissue *in vivo* will be anywhere from a factor 0.5 to 8 times what was assumed in these simulations.

The LTSRs utilized in these simulations are consistent with measurements reported for diseased and normal breast tissue [1, 2, 22]. These reports suggest that compression of the tissue results in considerable increases (a factor of 5) in the apparent Young's modulus of diseased tissue, but does not affect the Young's modulus of normal breast tissue [2]. For smaller lesions (0.5 cm diameter), rigid body motion was achieved for all of the LTSRs investigated. However, for the larger lesion, with an LTSR of 5, and to a lesser extent 10, rigid body motion was not achieved (Figures 10 and 12). Therefore, it may be useful to apply compression prior to Remote Palpation implementation.

Equation 1 indicates that increases in radiation force over that used in the simulations will occur with increases in absorption of tissue, decreases in the speed of sound in tissue, and increases in the intensity field generated by the transducer. In addition, a significant source of increased radiation force that is not modeled by Equation 1 is that of nonlinear propagation. Although Equation 1 does not indicate a dependence between pressure amplitude and radiation force, several researchers have demonstrated that there is an increase in radiation force associated with increasing pressure amplitude, due to nonlinear propagation [11, 19, 20]. For the same temporal average intensity, a wave with higher pressure amplitude and shorter pulse duration generates a larger radiation force than does a lower amplitude, longer duration wave. This is due to the higher order harmonics generated by nonlinear propagation, which result in an increase in absorption [11, 19, 26, 27]. We have observed

increases by a factor of 2.6 in breast applications *in vivo* [20]. For a thorough theoretical treatment of nonlinear enhancement of radiation force, the reader is referred elsewhere [11].

Nonlinear propagation could be incorporated into the model presented herein, by modifying Equation 1 [19, 27]:

$$F = \frac{2}{c} \sum_n \alpha_n * I_n, \tag{3}$$

where n represents the harmonic number. Thus, given an estimate of the intensity of each harmonic at a given point in space, the contribution of the energy in the harmonics can be accounted for. Incorporation of these effects would result in a nonlinear relationship between pressure amplitude and radiation force, in addition to modifying the shape of the intensity contours, due to the preferential generation of harmonics within the focal region [28, 29, 30, 31]. However, incorporation of these effects would not alter the linear relationship between force and displacement demonstrated in Figure 4.

The simulations were performed assuming a peak *in situ* intensity of 90 W/cm^2, which resulted in a peak displacements of 1.2 microns within 20 milliseconds for the linear-F/1 transducer. Given the linear relationship between displacement and force (Figure 4), and the desired peak displacement of at least 5 microns, four times this intensity is desirable (assuming the values used for absorption, sound speed and Young's modulus of tissue are valid). When the enhancing effects of nonlinear propagation are accounted for (an increase of 2.6), the required increase drops to 1.5 (or 135 W/cm^2).

There are two potential challenges associated with these intensity levels: 1) they exceed the FDA limit for diagnostic intensity levels, and 2) they may approach the maximum power output of currently available diagnostic scanners. The FDA currently limits the spatial peak temporal average intensity to 0.72 W/cm^2 *in situ*, in order to avoid potential tissue damage due to heating. However, this limit was determined assuming an indefinite application time. The simulations indicate that the force need only be applied for 5 milliseconds. Short duration, high intensity acoustic pulses were not foreseen in the development of the FDA limit. A more appropriate thermal safety indicator for this type of pulse can be determined using Equation 4, which predicts the temporal average intensity (I in W cm^{-2}) that would be required to generate a lesion, or burn, due to ultrasound exposure in a given time period (t, in seconds) [32]:

$$I = 10 * \sqrt{\frac{100}{t}}. \tag{4}$$

Assuming a 5 millisecond application time, 1400 W/cm^2 would be required to cause thermal

damage. This provides a safety factor of 10 over what may be required for Remote Palpation. However, Equation 4 is reported to be valid for frequencies in the low MHz range (*i.e.* less than 10 MHz). Given the increase in absorption associated with nonlinear propagation, it is likely that this temporal safety estimate will decrease due to harmonic generation. Under linear conditions, (*i.e.* neglecting the anticipated factor of 2.6 increase in radiation force from nonlinear propagation, thus requiring an intensity of 350 W/cm^2 for 5 msec) Equation 4 predicts a safety factor of 4.

The question of the maximum power output from diagnostic scanners is complex. Because the FDA limits are considerably lower than the maximum capacity of current diagnostic scanners, manufacturers do not quantify this parameter. After modifying the system software to remove the built-in safety features, we have measured spatial peak temporal average intensities from the 75L40 array on our Elegra scanner that correspond to *in vivo* values of 10.0 W/cm^2. Simulations indicate that the 2D 8x128 transducer will be capable of generating three times this amount (Table 1); only 4.5 times more power is required for Remote Palpation implementation. Development of diagnostic transducers capable of generating the required intensities seems plausible in the near future. Manufacturers are actively pursuing the development of more powerful diagnostic transducers for other applications, including harmonic and contrast imaging. The product of these efforts may be suitable for the clinical implementation of Remote Palpation.

Assuming the required force values can be achieved, the simulations indicate that Remote Palpation has considerable promise. Clear, quantifiable differences in displacement patterns exist in the presence or absence of lesions (Figures 9 through 12). The shape of the axial displacement profile for normal breast tissue using the linear-F/1 transducer is notable (Figure 12). The linear decrease in displacement along the axial extent of the profile results from the fact that as the tissue farther from the transducer is compressed, the proximal tissue is increasingly displaced to facilitate this motion. This linearly decreasing displacement profile is indicative of constant strain in this region, and is similar to profiles observed in elastography, where compression of the tissue is applied globally. This type of profile is not nearly as apparent for the 2D transducer (Figure 10), because in this case the axial extent of the radiation force field is much smaller (Figure 7).

Interestingly, a considerable increase in displacement occurs immediately proximal to a tissue/lesion interface when this interface lies within the radiation force field (Figure 12, 0.5 cm diameter lesion). This type of profile is consistent with those seen in elastography. In the

instance that the intensity field is completely contained within the lesion (*i.e.* Figure 12, 1.0 cm diameter lesion), the shape of the axial displacement profile does not differ considerably from that in normal tissue. However, in this case the magnitude of displacement is greatly decreased, thus comparison with surrounding tissue will indicate the presence of a lesion.

The implications of the assumptions made in the finite element analysis should not alter the trends observed herein. The temporal behavior of tissue may vary slightly due to the assumption of a numerically damped elastic medium, as opposed to a visco-elastic medium. The assumption of axial symmetry of the intensity field allowed accurate mesh generation of spatially complex intensity field contours while providing a three-dimensional solution. This could result errors in the estimation of the volume of the radiation force field in the elevation dimension for high f-number configurations. However, given that the lateral and elevation dimensions are an order of magnitude smaller than the axial dimension, this will have only a slight impact on the displacement profiles.

Conclusion

The simulations presented herein provide the framework for the design of a Remote Palpation imaging system. For a clinically relevant range of elastic moduli and lesion sizes, considerably different displacement patterns were generated. Peak displacements of several microns were observed. The forces required to generate these displacements are higher than those currently used in diagnostic ultrasound. They should not pose a danger to the patient due to their short duration, however, they may require the design of custom transducers. Most manufacturers are actively pursuing the development of more powerful diagnostic transducers, therefore it is plausible that future diagnostic transducers will be capable of generating the required forces.

The simulations indicate that a two-dimensional array is preferable to a linear array for the implementation of Remote Palpation. A 2D array provides more force, a smaller intensity field volume, and the ability to focus the intensity field in both the lateral and elevation dimensions. The displacement timing suggests that radiation force pushing beams should be applied for 5 milliseconds, and following this, tracking lines should be interspersed with pushing lines to avoid tissue relaxation during the tracking sequence. While further research is required to investigate the thermal and power issues, Remote Palpation as proposed herein appears to have considerable clinical potential.

Acknowledgments

This work was supported by DOD BCRP grant BC972755. We thank Altair Computing, Inc. for their considerable support with meshing and post-processing. We thank Siemens Medical Systems, Ultrasound Group for their guidance on system specifications. We thank Intel Corporation for their technical and in-kind support.

References

[1] A. Sarvazyan, A. Skovoroda, S. Emelianov, J. Fowlkes, J. Pipe, R. Adler, R. Buxton, and P. Carson, "Biophysical bases of elasticity imaging," *Acoustical Imaging*, vol. 21, pp. 223–240, 1995.

[2] T. Krouskop, T. Wheeler, F. Kallel, B. Garra, and T. Hall, "Elastic moduli of breast and prostate tissues under compression," *Ultrasonic Imaging*, vol. 20, pp. 260–274, 1998.

[3] Y. Yamakoshi, J. Sato, and T. Sato, "Ultrasonic imaging of internal vibration of soft tissue under forced vibration," *IEEE Trans. Ultrason., Ferroelec., Freq. Contr.*, vol. 17, no. 2, pp. 45–53, 1990.

[4] R. Lerner, S. Huang, and K. Parker, "Sonoelasticity images derived from ultrasound signals in mechanically vibrated tissues," *Ultrasound Med. Biol.*, vol. 16, pp. 231–239, 1990.

[5] K. Parker, S. Huang, R. Musulin, and R. Lerner, "Tissue response to mechanical vibrations for sonoelasticity imaging," *Ultrasound Med. Biol.*, vol. 16, pp. 241–246, 1990.

[6] T. Krouskop, D. Dougherty, and S. Levinson, "A pulsed doppler ultrasonic system for making noninvasive measurements of the mechanical properties of soft tissue," *J. Rehabil. Res. Dev.*, vol. 24, pp. 1–8, 1987.

[7] S. Levinson, "Ultrasound propagation in anisotropic soft tissues, the application of linear elastic theory," *J. Biomech.*, vol. 20, pp. 251–260, 1987.

[8] J. Ophir, I. Cespedes, H. Ponnekanti, Y. Yazdi, and X. Li, "Elastography: A quantitative method for imaging the elasticity of biological tissues," *Ultrasonic Imaging*, vol. 13, pp. 111–134, 1991.

[9] M. O'Donnell, A. Skovoroda, B. Shapo, and S. Emelianov, "Internal displacement and strain imaging using ultrasonic speckle tracking," *IEEE Trans. Ultrason., Ferroelec., Freq. Contr.*, vol. 41, pp. 314–325, 1994.

[10] L. Gao, K. Parker, R. Lerner, and S. Levinson, "Imaging of the elastic properties of tissue - a review," *Ultrasound Med. Biol.*, vol. 22, no. 8, pp. 959–977, 1996.

[11] A. Sarvazyan, O. Rudenko, S. Swanson, J. Fowlkes, and S. Emelianov, "Shear wave elasticity imaging: A new ultrasonic technology of medical diagnostics," *Ultrasound Med. Biol.*, vol. 24, no. 9, pp. 1419–1435, 1998.

[12] W. Walker, "Internal deformation of a uniform elastic solid by acoustic radiation force," *J. Acoust. Soc. Am.*, vol. 105, no. 4, pp. 2508–2518, 1999.

[13] T. Sugimoto, S. Ueha, and K. Itoh, "Tissue hardness measurement using the radiation force of focused ultrasound," in *Proceedings of the 1990 Ultrasonics Symposium*, pp. 1377–1380, 1990.

[14] K. Nightingale, R. Nightingale, T. Hall, and G. Trahey, "The use of radiation force induced tissue displacements to image stiffness: a feasibility study." 23rd International Symposium on Ultrasonic Imaging and Tissue Characterization, May 27-29, 1998.

[15] M. Fatemi and J. Greenleaf, "Ultrasound-stimulated vibro-acoustic spectrography," *Science*, vol. 280, pp. 82–85, 1998.

[16] G. Torr, "The acoustic radiation force," *Am. J. Phys.*, vol. 52, pp. 402–408, 1984.

[17] W. Nyborg, "Acoustic streaming," in *Physical Acoustics* (W. Mason, ed.), vol. IIB, ch. 11, pp. 265–331, New York: Academic Press Inc, 1965.

[18] D. Dalecki, *Mechanisms of Interaction of Ultrasound and Lithotripter Fields with Cardiac and Neural Tissues.* PhD thesis, University of Rochester, 1993.

[19] H. Starritt, F. Duck, and V. Humphrey, "Forces acting in the direction of propagation in pulsed ultrasound fields," *Phys. Med. Biol.*, vol. 36, pp. 1465–1474, 1991.

[20] K. Nightingale, P. Kornguth, and G. Trahey, "The use of acoustic streaming in breast lesion diagnosis: a clinical study," *Ultrasound Med. Biol.*, vol. 25, no. 1, pp. 75–87, 1999.

[21] J. Jensen and N. Svendsen, "Calculation of pressure fields from arbitrarily shaped, apodized, and excited ultrasound transducers," *IEEE Trans. Ultrason., Ferroelec., Freq. Contr.*, vol. 39, pp. 262–267, 1992.

[22] A. Skovoroda, A. Klishko, D. Gusakyan, Y. Mayevskii, V. Yermilova, G. Oranskaya, and A. Sarvazyan, "Quantitative analysis of the mechanical characteristics of pathologically changed soft biological tissues," *Biophysics*, vol. 40, no. 6, pp. 1359–1364, 1995.

[23] Y. Zhu, P. Chaturvedi, and M. Insana, "Strain imaging with a deformable mesh," *Ultrasonic Imaging*, vol. 21, no. 2, pp. 127–146, 1999.

[24] G. Trahey, J. Allison, and O. Vonramm, "Angle independent ultrasonic detection of blood flow," *IEEE Trans. Biomed. Egr.*, vol. BME-34, no. 12, pp. 965–967, 1987.

[25] W. Walker and G. Trahey, "A fundamental limit on delay estimation using partially correlated speckle signals," *IEEE Trans. Ultrason., Ferroelec., Freq. Contr.*, vol. 42, no. 2, pp. 301–308, 1995.

[26] O. Rudenko, S. A., and S. Emelianov, "Acoustic radiation force and streaming induced by focused nonlinear ultrasound in a dissipative medium," *J. Acoust. Soc. Am.*, vol. 99, no. 5, pp. 2791–2798, 1996.

[27] D. Dalecki, E. Carstensen, K. Parker, and D. Bacon, "Absorption of finite amplitude focused ultrasound," *J. Acoust. Soc. Am.*, vol. 89, no. 5, pp. 2435–2447, 1991.

[28] G. Wojcik, J. Mould, S. Ayter, and L. Carcione, "A studey of second harmonic generation by focused medical transducer pulses," in *Proceedings of the 1998 IEEE Ultrasonics Symposium*, 1998.

[29] M. Averkiou, D. Roundhill, and J. Powers, "A new imaging technique based on the nonlinear properties of tissues," in *Proceedings of the 1997 IEEE Ultrasonics Symposium*, pp. 1561–1566, 1997.

[30] B. Ward, A. Baker, and V. Humphrey, "Nonlinear propagation applied to the improvement of resolution in diagnostic medical ultrasound," *J. Acoust. Soc. Am.*, vol. 101, no. 1, pp. 143–154, 1997.

[31] T. Christopher, "Finite amplitude distortion-based inhomogeneous pulse echo ultrasonic imaging," *IEEE Trans. Ultrason., Ferroelec., Freq. Contr.*, vol. 44, no. 1, pp. 125–139, 1997.

[32] AIUM Bioeffects Committee, "Bioeffects considerations for the safety of diagnostic ultrasound," *J. Ultrasound Med.*, vol. 7, no. 9, Supplement, 1988.

Configuration	Scale Factor
2D	3.23
Linear-F/1	1.00
Linear-F/1.5	0.54
Linear-F/2	0.33
Linear-F/2.5	0.23
Linear-F/3	0.17

Table 1: Normalized peak intensity values for each transducer configuration. The higher the f-number, the fewer the elements; thus for the linear transducer lower f-numbers have larger scale factors. The 2D array has more total surface area than any of the linear configurations, and thus it has the largest scale factor.

Figure 1: Simulated contours of constant temporal average intensity generated by FIELD_II. The transducer is on the left side of the page. This plot also portrays two lesion boundaries (0.5 and 1.0 cm diameter, the dashed lines). The intensity field values of the contours were normalized to the peak value; contours represent levels of 0.9, 0.5, and 0.1 the peak value. After meshing, these contours were 'spun' about the x (axial) axis to generate a three dimensional mesh.

Figure 2: Top: Finite element mesh used for the linear transducer. The transducer is on the left (back) side of the page, with its axial dimension along the central axis of the mesh. This mesh was generated by first meshing the contours shown in Figure 1, and then spinning that mesh 90 degrees about its x-axis. The diameter of the resulting hemisphere is 5 cm, and is intended to represent an effectively infinite boundary condition. This mesh was constrained on the distal quarter of the surface of the hemisphere (the right (front) side of the page), in order to simulate a breast resting on a concave table, opposite the transducer. Bottom: This is a magnified version of the central plane of the mesh, showing the the increased element density in the focal region, the radiation force field contours for the linear-F/1 transducer configuration, and the outline of a spherical 1.0 cm diameter lesion.

Figure 3: Displacements resulting from radiation force application using the 2D transducer. The top row illustrates displacements across the entire mesh, whereas the middle row shows only the center 2 cm. The contour levels in the middle row range from 0.3 to 2.8 microns, in increments of 0.06 microns. The bottom row provides quantitative displacement values along the central axis of the transducer. The transducer is on the left side of these images. Left column: Displacement pattern in normal breast tissue (Young's modulus of 10 kPa) after 20 milliseconds of force application. Right column: Corresponding displacement images in the presence of a 0.5 cm diameter lesion with a Young's modulus of 400 kPa. The location of the lesion has been highlighted in gray.

Figure 4: Peak axial displacement for different radiation force levels assuming a Linear-F/1 transducer configuration and normal breast tissue with a Young's modulus of 10kPa.

Figure 5: Top: Axial displacement along the central axis versus stiffness of normal breast tissue, assuming a Linear-F/1 transducer configuration. Bottom: Breast stiffness versus the inverse of the peak displacement, at 20 msec after the initiation of radiation force application.

Figure 6: Magnified view of contours of displacement (dashed lines) in normal breast tissue (E=10kPa), for the 2D transducer (top), and the Linear-F/1 transducer configuration (bottom). The outer boundary of the associated intensity field (*i.e.* the 0.1 level contour of the intensity field) is superimposed on each figure as a solid black line. The contours are normalized; each level represents a 10% decrease in displacement from the maximum. Note that the shape of the displacement contours are similar to the shape of the intensity fields: the 2D contours are more symmetric about the focus, whereas the Linear-F/1 contours exhibit an asymmetry along the axial dimension, with larger displacements occurring in front of the focus (*i.e.* closer to the transducer on the left side of the page).

Figure 7: Outer boundary of the radiation force fields for different transducer configurations (*i.e.* the 0.1 level contours of the intensity fields). Note that the 2D boundary covers a much smaller volume than the others, and that the 2D, F/1 and F/1.5 boundaries are considerably more saddle-like than the higher f-numbers. Note also the different scales on the two axes.

Figure 8: Displacement along the central axis of the tissue versus transducer f-number, assuming normal breast tissue with a Young's modulus of 10 kPa.

Figure 9: Contours of displacement for different lesion sizes and stiffnesses using the 2D transducer. The contour levels range from 0.3 to 2.8 microns, in increments of 0.06 microns. The Young's modulus of normal breast tissue is 10 kPa. In the cases where a lesion is present, its shape has been highlighted in gray. Displacement values are quantified in Figure 10.

Figure 10: Axial displacement along the central axis of the 2D transducer for different lesion sizes and stiffnesses corresponding to the results in Figure 9. The Young's modulus of normal breast tissue is 10 kPa, and the lesion diameters are 0.5 and 1.0 cm with varying Young's moduli (50, 100 and 400 kPa). The legend notation indicates lesion diameter (cm)/lesion Young's modulus (kPa).

Figure 11: Contours of displacement for different lesion diameters and stiffnesses using the linear transducer in an F/1 configuration. The contour levels range from 0.3 to 1.2 microns, in increments of 0.03 microns. The Young's modulus of normal breast tissue is 10 kPa. In the cases where a lesion is present, its shape has been highlighted in gray. Displacement values are quantified in Figure 12.

Figure 12: Axial displacement along the central axis of the linear-F/1 transducer for different lesion sizes and stiffnesses corresponding to the results in Figure 11. The Young's modulus of normal breast tissue is 10 kPa, and the lesion diameters are 0.5 and 1.0 cm with varying Young's moduli (50, 100 and 400 kPa). The legend notation indicates lesion diameter (cm)/lesion Young's modulus (kPa). The axial extent of the radiation force field is larger than the lesion diameter in the case of the 0.5 cm diameter lesion, which results in large displacements immediately in front of the lesion.

Figure 13: Top: Displacement along the central axis of the linear-F/1 transducer in normal breast tissue (Young's modulus 10kPa) through time. Bottom: Displacement at the focal point of the linear-F/1 transducer (*i.e.* x=0 on the top plot) through time for different types of tissue. Note that although the ramp up time varies, after 20 msec each case is near its steady state displacement.

Figure 14: Normalized displacement at the focal point of the linear-F/1 transducer through time for normal breast tissue of different Young's moduli. The force function in this simulation was a ramp up in 2 msec, held for 20 msec, and then turned off. These simulations were run without damping.

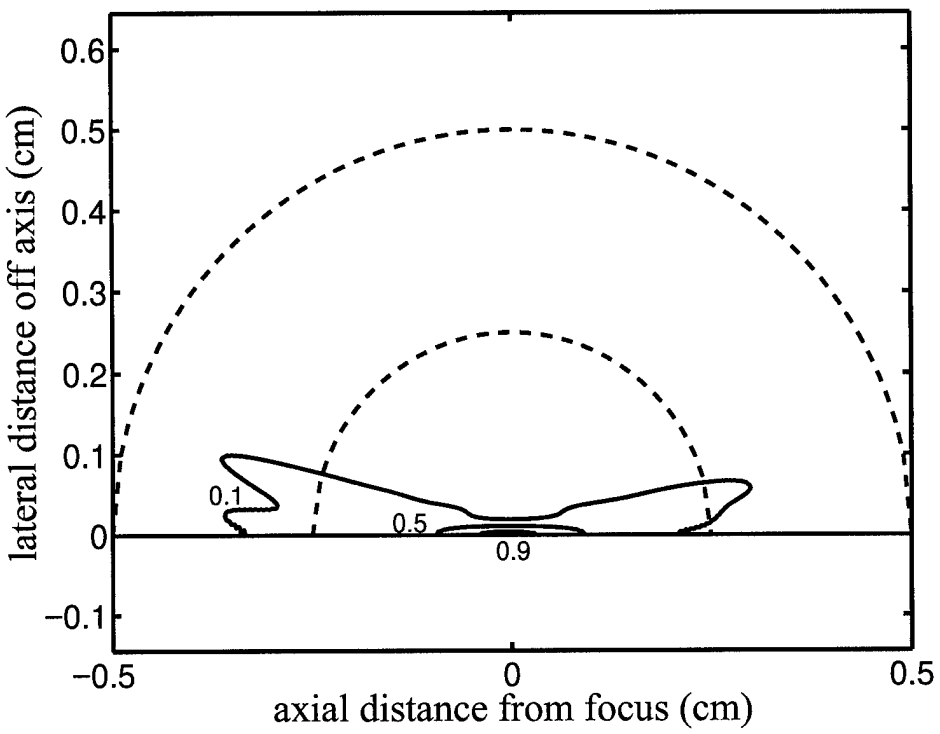
0.6
0.5
0.4
0.3
0.2
0.1
0
−0.1
lateral distance off axis (cm)
0.1
0.5
0.9
−0.5
0
0.5
axial distance from focus (cm)

Figure 1:

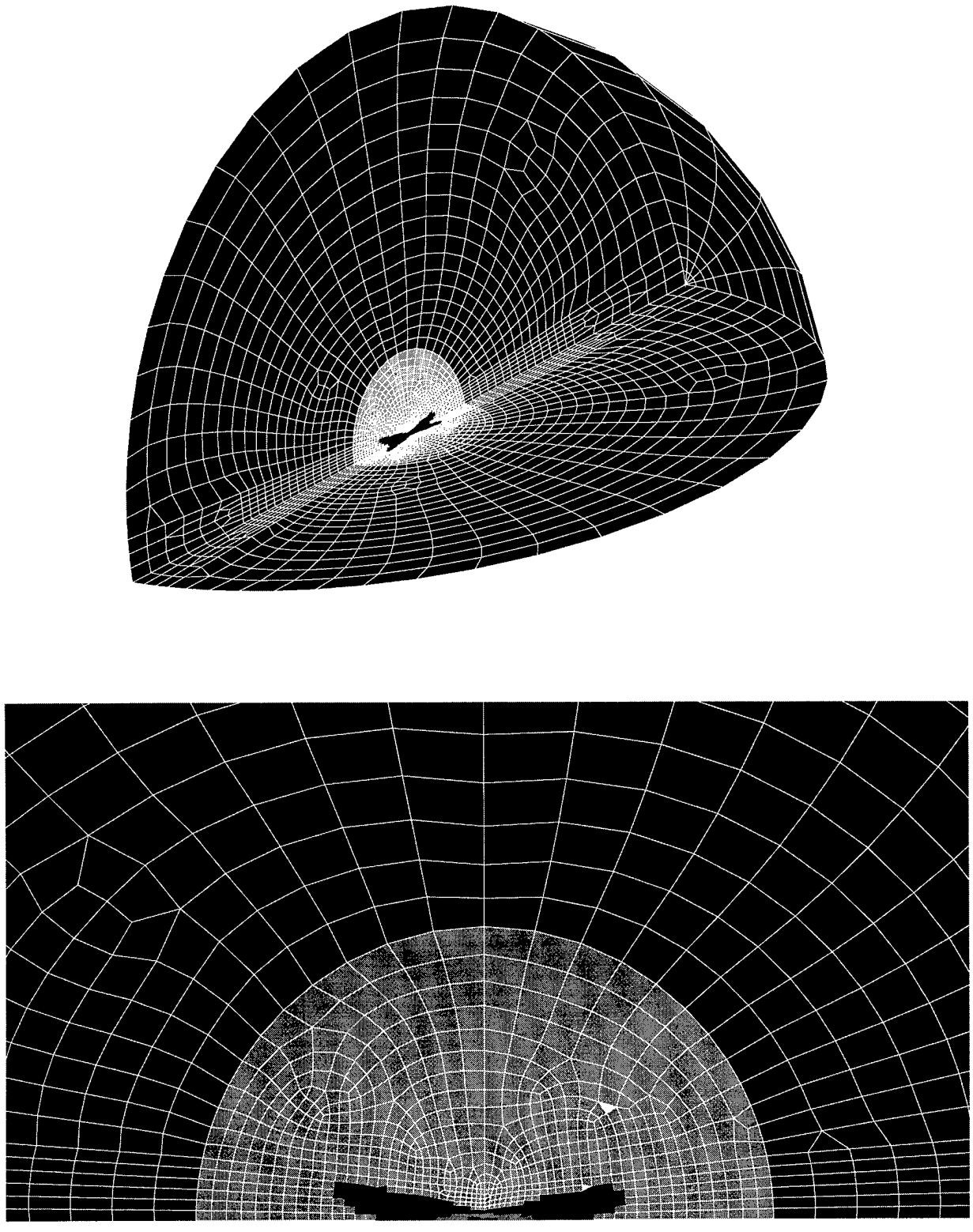

Figure 2:

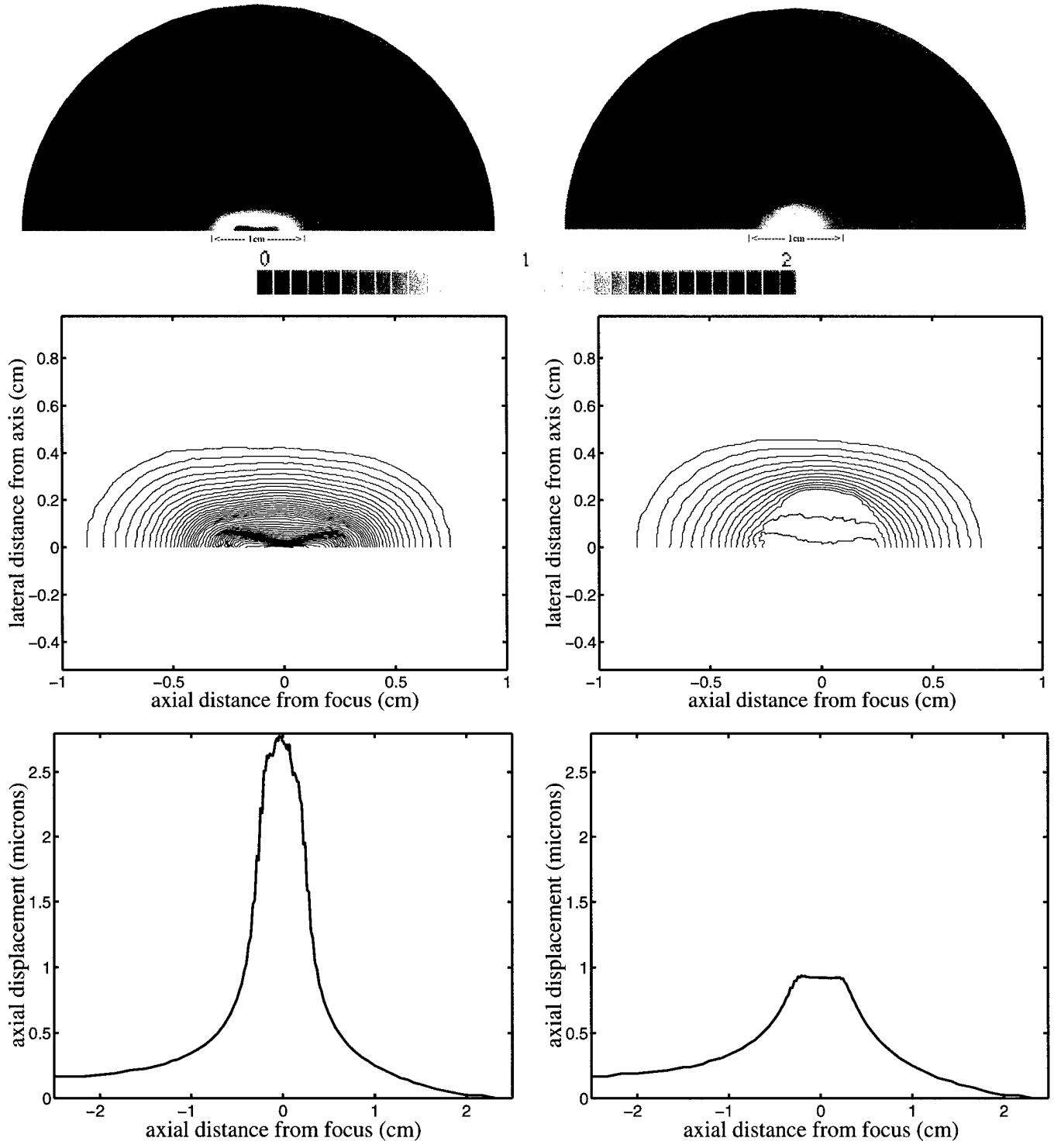
1cm
1cm
0
1
2
lateral distance from axis (cm)
axial distance from focus (cm)
lateral distance from axis (cm)
axial distance from focus (cm)
axial displacement (microns)
axial distance from focus (cm)
axial displacement (microns)
axial distance from focus (cm)

Figure 3:

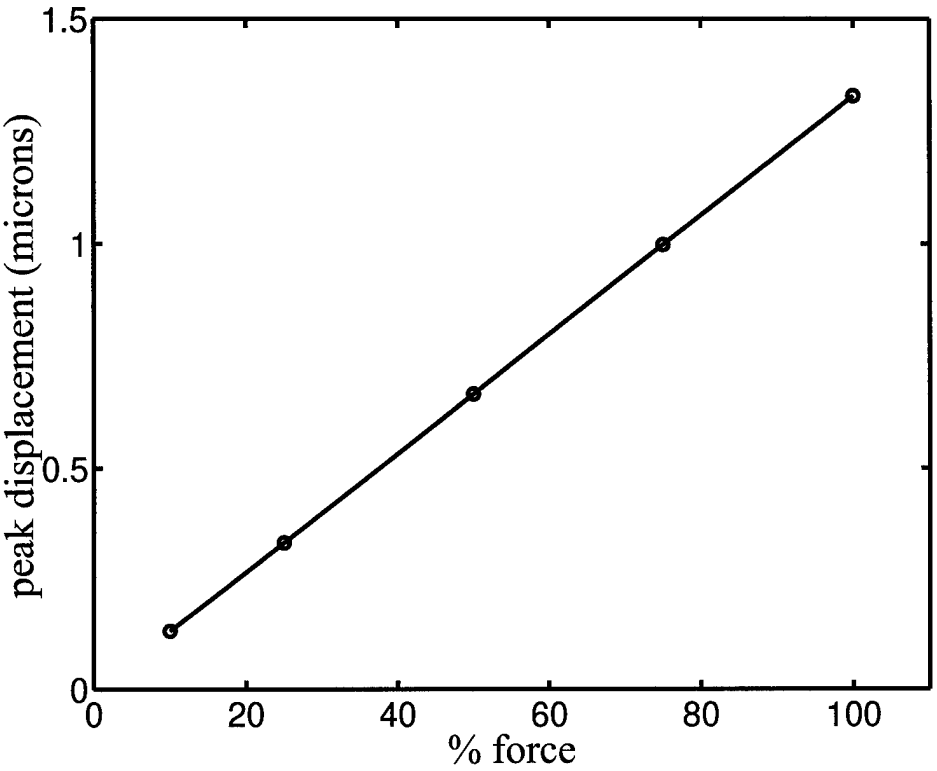

Figure 4:

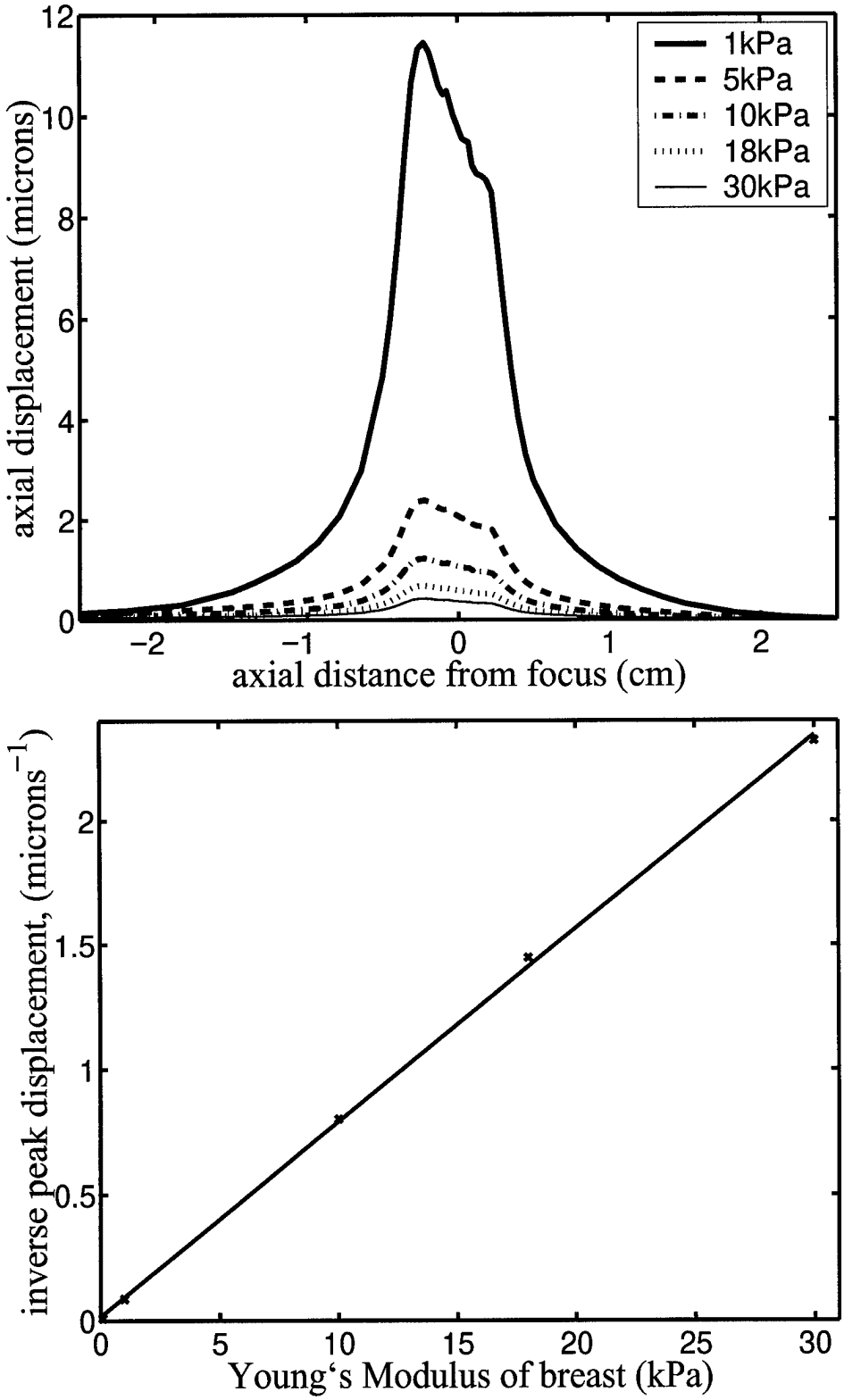
1kPa
5kPa
10kPa
18kPa
30kPa
axial displacement (microns)
axial distance from focus (cm)
inverse peak displacement, (microns^{-1})
Young's Modulus of breast (kPa)

Figure 5:

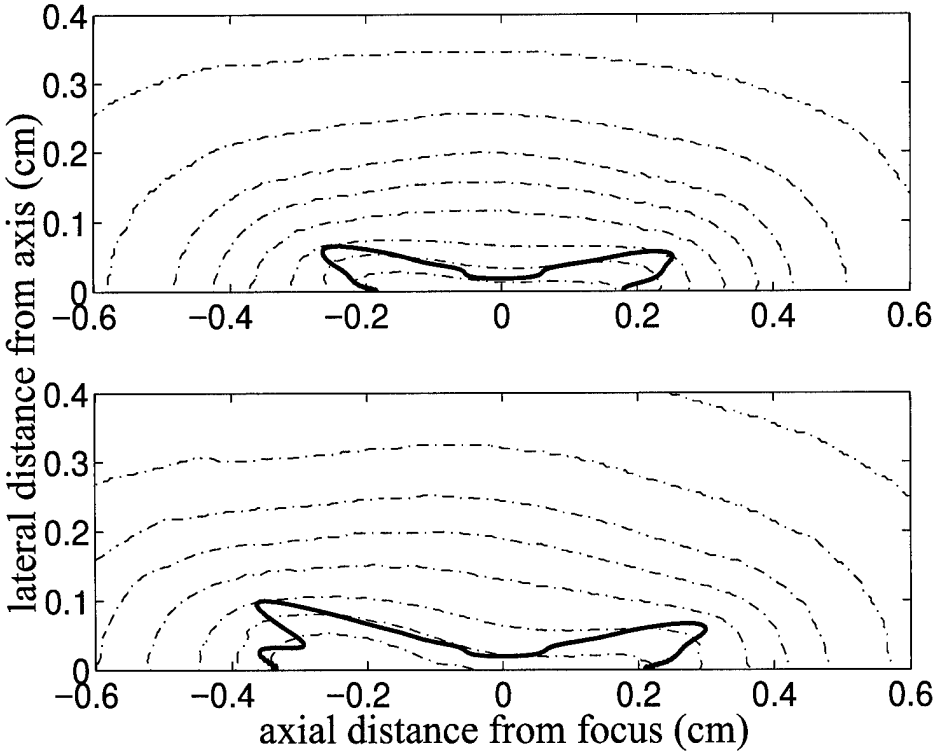

Figure 6:

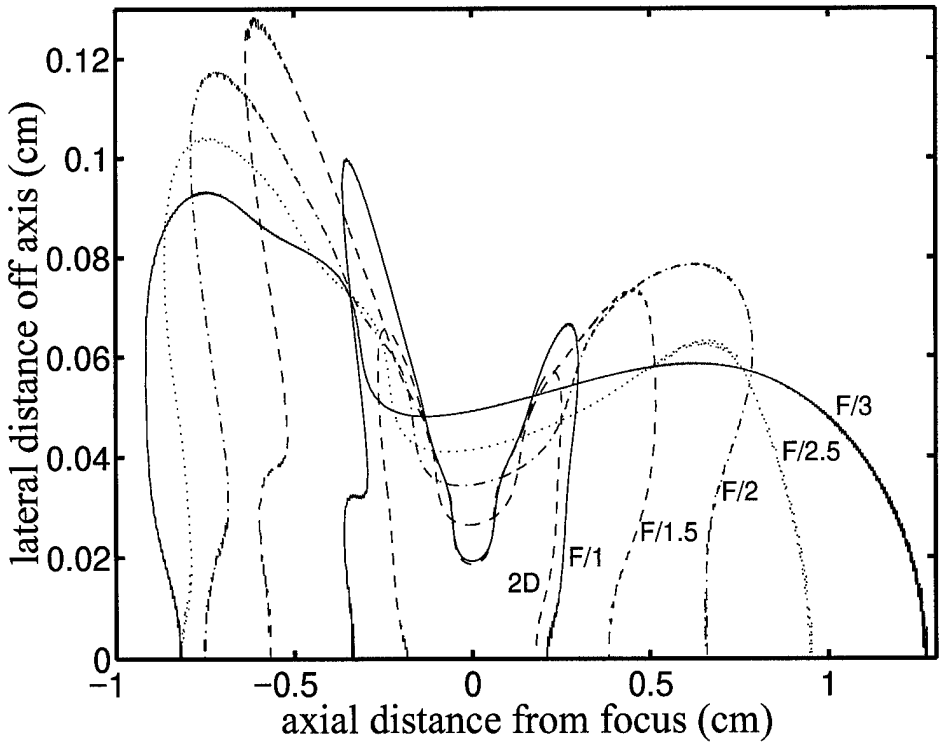

Figure 7:

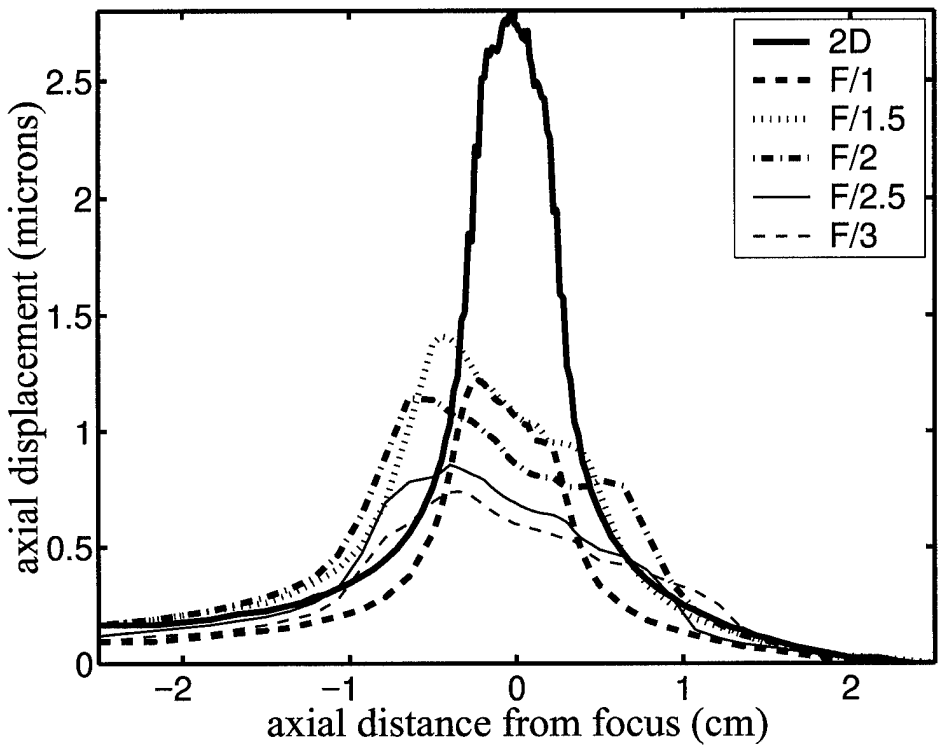
2D
F/1
F/1.5
F/2
F/2.5
F/3
axial displacement (microns)
axial distance from focus (cm)
0
0.5
1
1.5
2
2.5
−2
−1
0
1
2

Figure 8:

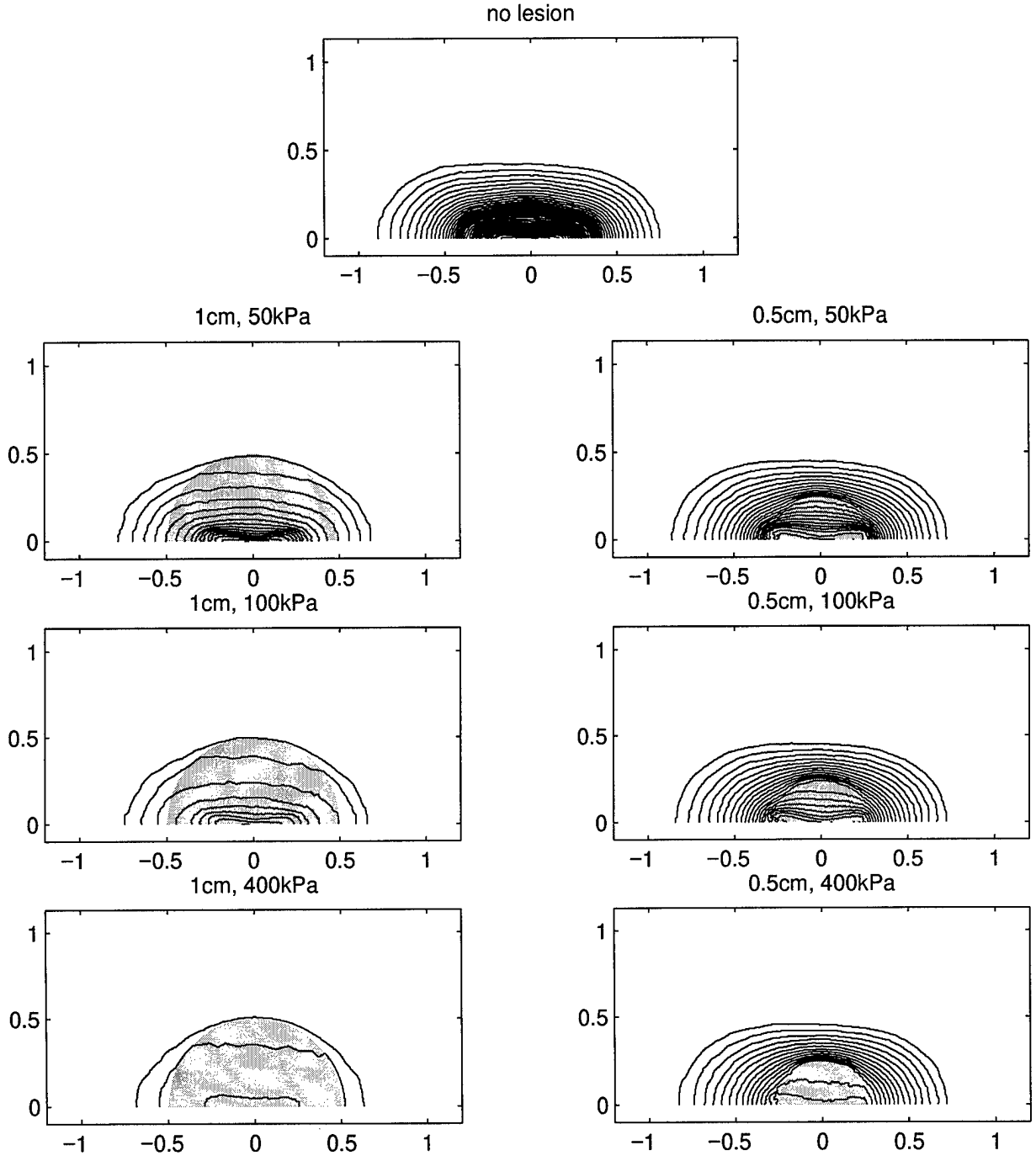
no lesion
1cm, 50kPa
0.5cm, 50kPa
1cm, 100kPa
0.5cm, 100kPa
1cm, 400kPa
0.5cm, 400kPa

Figure 9:

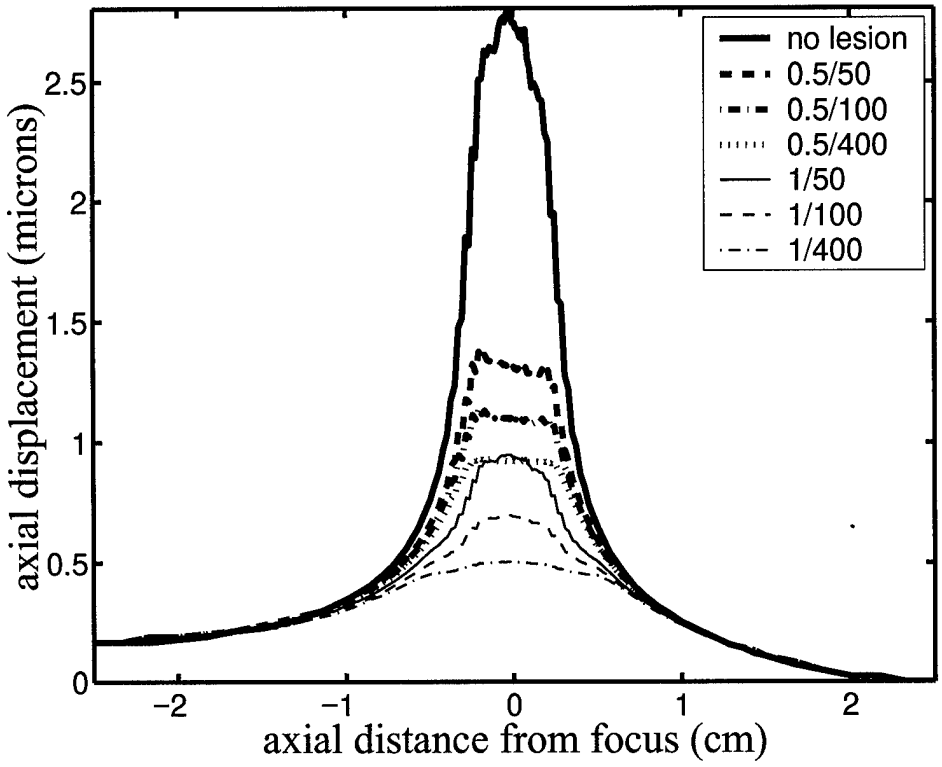
no lesion
0.5/50
0.5/100
0.5/400
1/50
1/100
1/400
axial displacement (microns)
axial distance from focus (cm)
0
0.5
1
1.5
2
2.5
−2
−1
0
1
2

Figure 10:

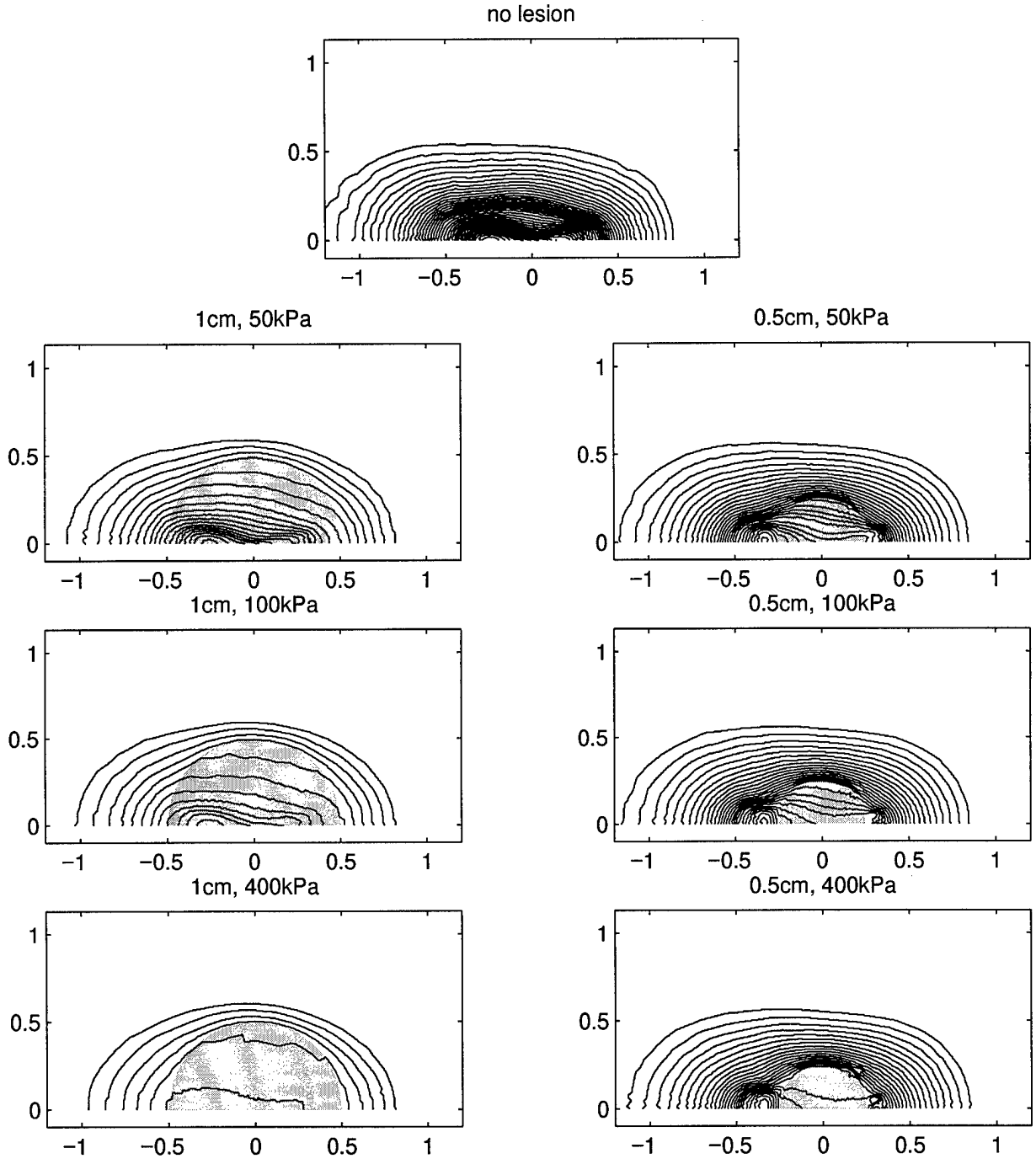
no lesion
1cm, 50kPa
0.5cm, 50kPa
1cm, 100kPa
0.5cm, 100kPa
1cm, 400kPa
0.5cm, 400kPa

Figure 11:

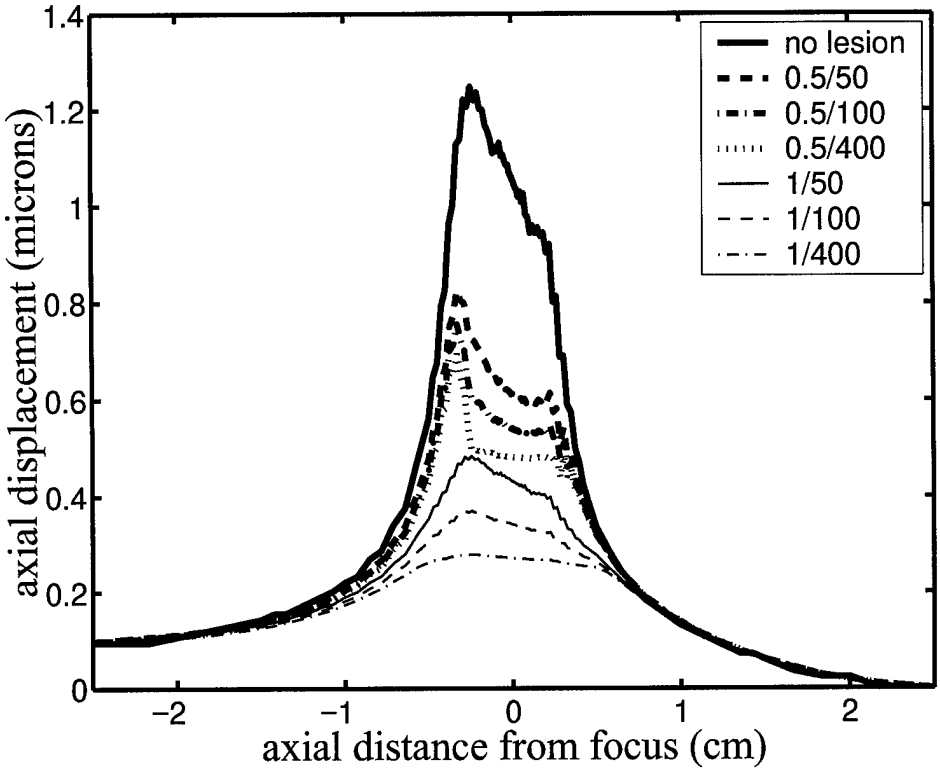
1.4
1.2
1
0.8
0.6
0.4
0.2
0
−2
−1
0
1
2
axial displacement (microns)
axial distance from focus (cm)
no lesion
0.5/50
0.5/100
0.5/400
1/50
1/100
1/400

Figure 12:

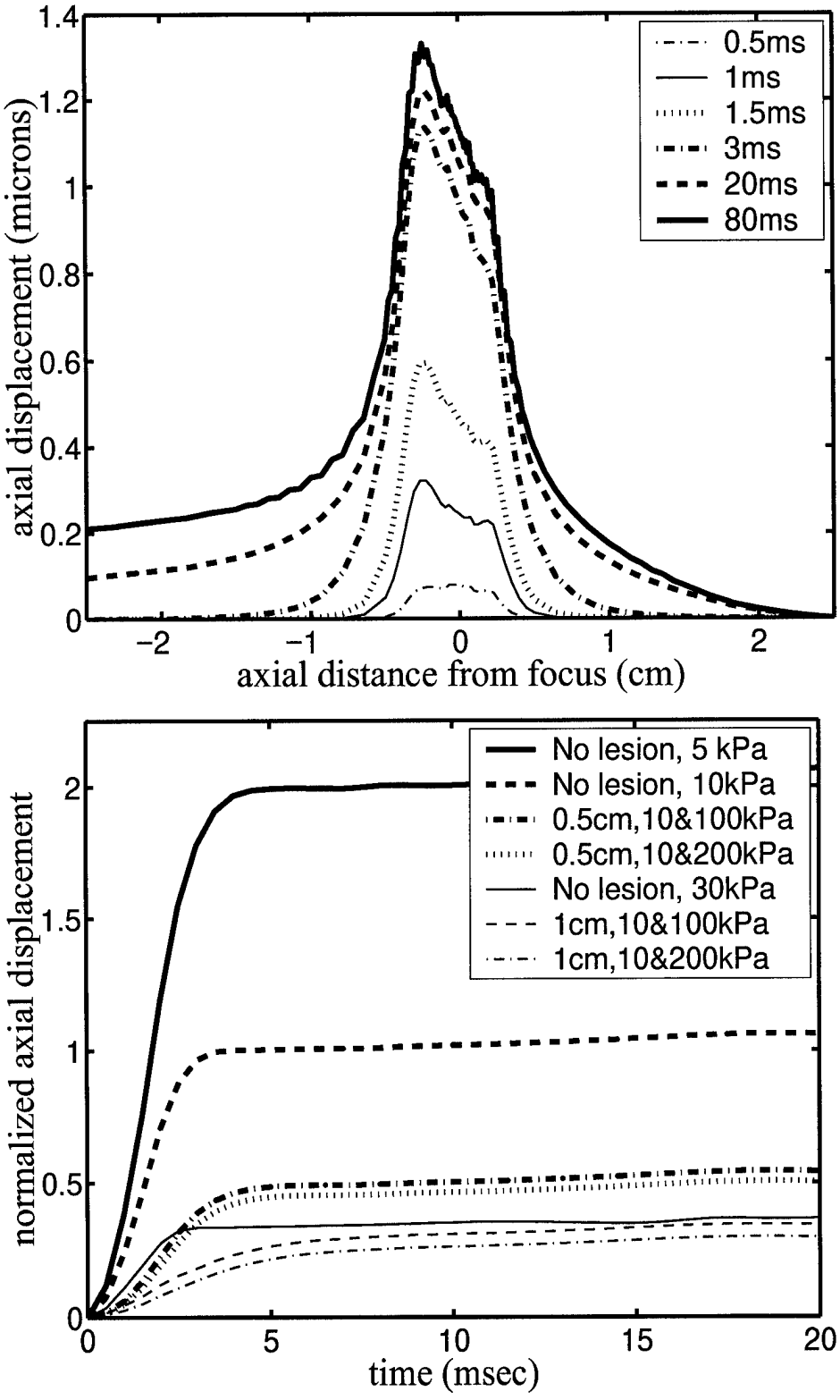
0.5ms
1ms
1.5ms
3ms
20ms
80ms
axial displacement (microns)
axial distance from focus (cm)
No lesion, 5 kPa
No lesion, 10kPa
0.5cm,10&100kPa
0.5cm,10&200kPa
No lesion, 30kPa
1cm,10&100kPa
1cm,10&200kPa
normalized axial displacement
time (msec)

Figure 13:

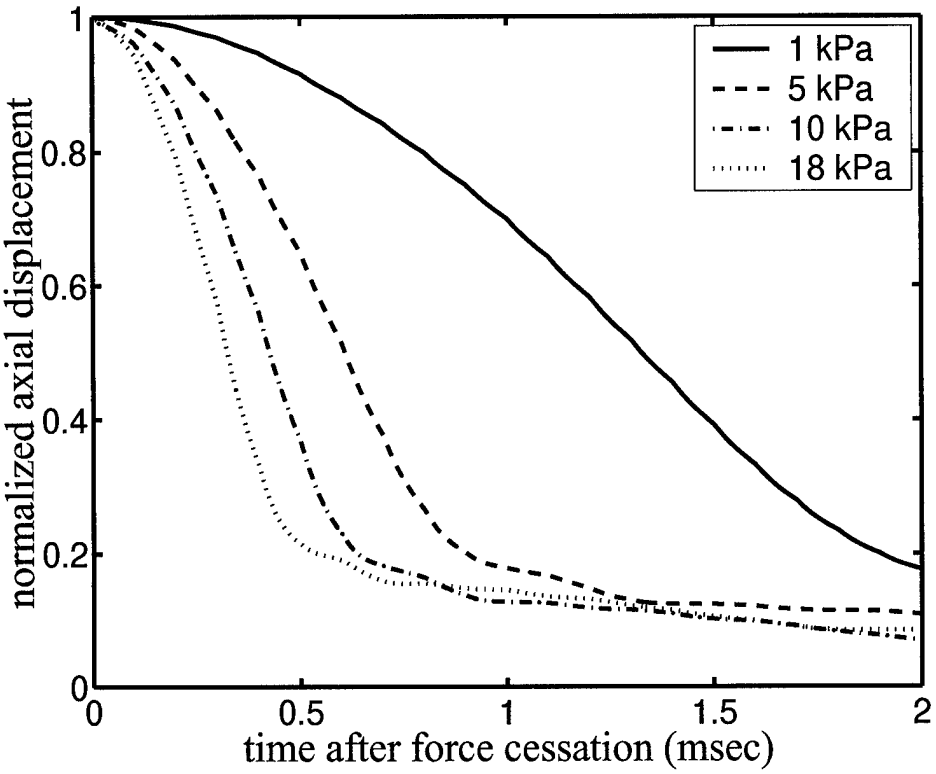
1 kPa
5 kPa
10 kPa
18 kPa
normalized axial displacement
time after force cessation (msec)
0
0.2
0.4
0.6
0.8
1
0
0.5
1
1.5
2

Figure 14: